Journal of Biomedical Optics 9(4), 700–710 (July/August 2004)

Estimation of melanin and hemoglobin in skin tissue using multiple regression analysis aided by Monte Carlo simulation

Izumi Nishidate
Muroran Institute of Technology
Division of Science for Composite Functions
27-1 Mizumoto-cho
Muroran 050-8585
Japan

Yoshihisa Aizu
Hiromichi Mishina
Muroran Institute of Technology
Department of Mechanical Systems Engineering
27-1 Mizumoto-cho
Muroran 050-8585
Japan
E-mail: aizu@mmm.muroran-it.ac.jp

Abstract. To estimate the concentrations of melanin and blood and the oxygen saturation in human skin tissue, we propose a method using a multiple regression analysis aided by a Monte Carlo simulation for diffuse reflectance spectra from the skin tissue. By using the absorbance spectrum as a response variable and the extinction coefficients of melanin, oxygenated hemoglobin, and deoxygenated hemoglobin as predictor variables, the multiple regression analysis gives regression coefficients. The concentrations of melanin and blood are determined from the regression coefficients using conversion vectors that are estimated numerically in advance, while the oxygen saturation is obtained directly from the regression coefficients. Numerical and experimental investigations were performed for layered skin tissue models and phantoms. Measurements of human skin were also carried out to monitor variations in the melanin and blood contents and oxygenation during cuff occlusion. The results confirmed the usefulness of the proposed method. © *2004 American Institute of Physics.* [DOI: 10.1117/1.1756918]

Keywords: skin tissue; oxygen saturation; hemoglobin; melanin; multiple regression analysis; diffuse reflectance; Monte Carlo simulation; absorbance.

Paper 03080 received Jun. 16, 2003; revised manuscript received Oct. 24, 2003; accepted for publication Oct. 24, 2003

1 Introduction

Various optical methods[1–6] have been reported for effective and noninvasive medical diagnostics of living human skin tissue. Quantitative estimation of the melanin and blood concentrations and blood oxygenation is important for detecting various skin diseases, including cancers; monitoring health status and tissue metabolism; and evaluating convalescence. The major chromophores in the superficial skin layer are melanin, oxygenated hemoglobin, and deoxygenated hemoglobin, which show distinctive optical absorption properties in the visible wavelength range. If the concentration of each chromophore varies, then the corresponding change may be visible in light diffusely reflected from the skin tissue in this wavelength range. Therefore, analysis of the diffuse reflectance spectra may provide us with useful information on tissue activities that are related to melanin and hemoglobin. On the other hand, the diffuse reflectance spectra also depend on the light scattering that is due to the structures of tissues and cells, such as collagen fibers and other cellular structures. Thus, estimation of the melanin and hemoglobin concentrations requires knowledge of the scattering properties of light in skin tissue as well as its absorption properties.

A number of spectroscopic methods have been studied for noninvasive determination of the scattering and absorption properties in living tissues, including time-resolved measurements,[7] a frequency-domain method,[8] and spatially resolved measurements.[9–13] Chemometrics is generally known as a useful means for data analysis in spectroscopy. Some methods using this approach have been studied for skin tissue spectroscopy also to evaluate absorbing components in the tissue. Tsumura et al.[14] proposed a method using an independent component analysis of color images for visualizing the spatial distributions of melanin and hemoglobin in human skin. Shimada et al.[15] reported a method for predicting absorption spectra of skin tissue using multiple regression analysis based on the modified Lambert-Beer law. This method is simple and seems to be promising for routine assessments of melanin and hemoglobin concentrations in skin tissue because of assuming the modified Lambert-Beer law. However, reliable and absolute measurements are still difficult with this method because of the nonlinearity between the absorbance and the concentration of chromophores. Owing to this problem, the measurable range of concentration changes is limited and an estimation of oxygen saturation has not yet been made using their method.

In this paper we propose a different approach to using multiple regression analysis to estimate the concentrations of melanin and hemoglobin together with the oxygen saturation in skin tissue. In the proposed method, the nonlinearity between the absorbance of skin tissue and the concentration of each chromophore is compensated by conversion vectors derived in advance from a number of absorbance spectra simulated by the Monte Carlo method for various values of the melanin and hemoglobin concentrations. The possibility of

Address all correspondence to Dr. Yoshihisa Aizu, Muroran Institute of Technology, Department of Mechanical Systems Engineering, 27-1 Mizumoto-cho, Muroran 050-8585, Japan. Tel: 81 143 46 5348; Fax: 81 143 46 5360; E-mail: aizu@mmm.muroran-it.ac.jp

1083-3668/2004/$15.00 © 2004 SPIE

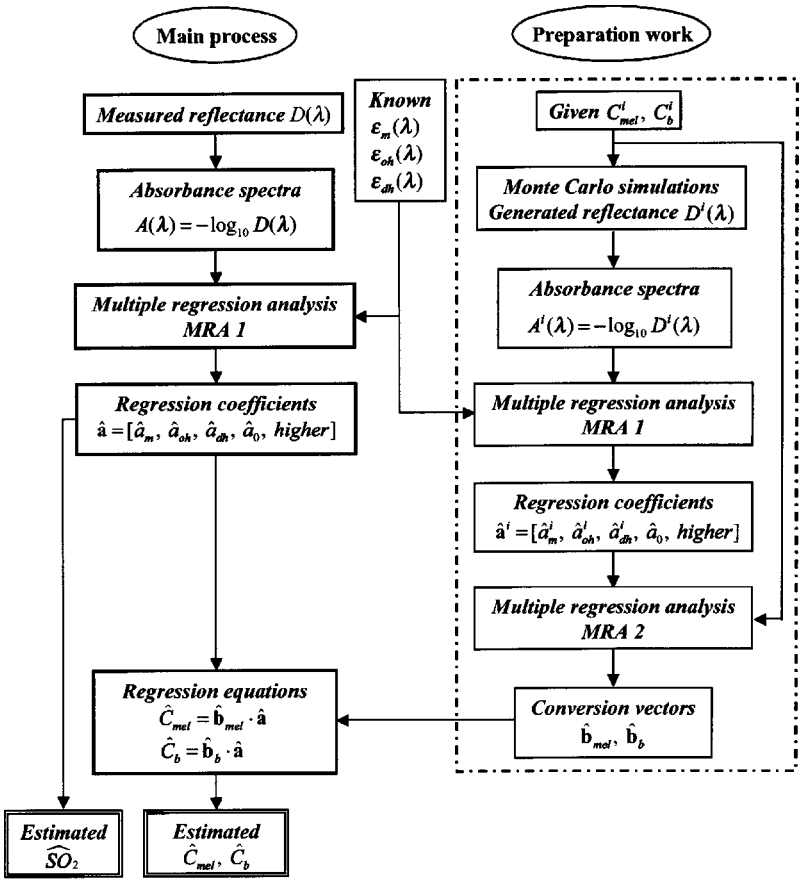

Fig. 1 Flow chart of the estimation process.

this method was numerically investigated for absorbance spectra generated with typical optical parameters of human skin. Experiments with two-layered skin tissue phantoms and *in vivo* measurements for human skin during cuff occlusion were performed to confirm the usefulness of the method.

2 Theory

2.1 *Multiple Regression Analysis*

In multiple regression analysis, a relationship between two variable sets $y_k(k=1,2,...,p)$ and $x_{jk}(j=1,2,...,q)$ is assumed to be given by the following linear equation,

$$y_k = \alpha_0 + \sum_{j=1}^{q} \alpha_j \times x_{jk} + e_k , \tag{1}$$

where y_k and x_{jk} represent response variables and predictor variables, respectively, α_0 is a constant component, and e_k expresses unknown error components. In this multiple regression model, p is the number of sample data being analyzed and q is that of predictor variables. The regression coefficients $\alpha_j(j=0,1,2,\cdots,q)$ are unknown values that are estimated by the method of least-squares in the analysis. Let us denote the estimated regression coefficients by $\hat{\alpha}_j$; then the corresponding multiple regression equation is expressed as

$$\hat{y}_k = \hat{\alpha}_0 + \sum_{j=1}^{q} \hat{\alpha}_j \times x_{jk} , \tag{2}$$

$$y_k = \hat{y}_k + r_k \tag{3}$$

where $\hat{y}_k$ are the response variables estimated using $\hat{\alpha}_j$, and r_k is the residual. A measure for suitability of the regression equation is given by the parameter R^2, which is defined as the square of the multiple correlation coefficient R, that is,

$$R^2 = \left[\frac{\Sigma_k (y_k - \overline{y_k})(\hat{y}_k - \overline{\hat{y}_k})}{\sqrt{\Sigma_k (y_k - \overline{y_k})^2} \sqrt{\Sigma_k (\hat{y}_k - \overline{\hat{y}_k})^2}} \right]^2 , \tag{4}$$

where $\overline{y_k}$ and $\overline{\hat{y}_k}$ denote the average of y_k and $\hat{y}_k$, respectively, over the p number of data. The value of R is the correlation coefficient between y_k and $\hat{y}_k$. The value of R^2 ranges from 0 to 1, and the linear approximation becomes better as R^2 approaches 1.

2.2 *Multiple Regression Model for Modified Lambert-Beer Law*

Figure 1 shows a flow chart of the proposed method. For a semi-infinite scattering medium such as human skin, an absorbance spectrum $A(\lambda)$ is defined as

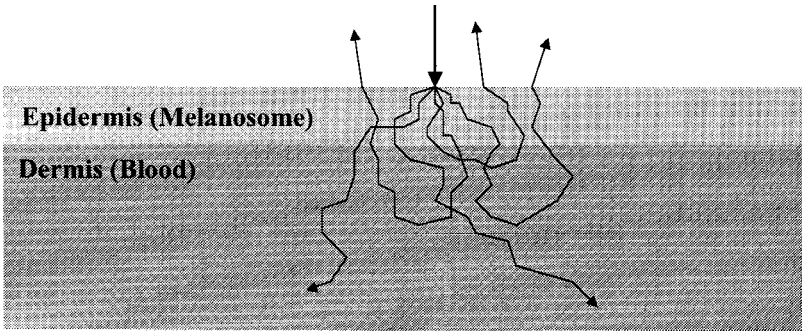

Fig. 2 Two-layered skin tissue model.

$$A(\lambda) = -\log_{10} D(\lambda), \tag{5}$$

where $D(\lambda)$ is a reflectance spectrum obtained from the medium and λ is its wavelength. According to the modified Lambert-Beer law,[16,17] the absorbance spectrum of a homogeneous scattering medium containing an absorber is expressed as

$$A(\lambda) = C \times \overline{l}(\lambda, C) \times \varepsilon(\lambda) + S(\lambda), \tag{6}$$

where C and $\varepsilon(\lambda)$ are the molar concentration and molar extinction coefficient of the absorber, respectively, $\overline{l}(\lambda, C)$ is the mean path length, and $S(\lambda)$ is attenuation that is due to scattering. Considering that the upper part of the skin tissue mainly consists of epidermis containing the melanin and dermis containing the oxygenated and deoxygenated hemoglobin, the absorbance spectrum may be given by the sum of the absorbance of epidermis, $A_{epi}(\lambda)$, that of dermis, $A_{der}(\lambda)$, and attenuation by scattering, $S(\lambda)$ as the following equation:[16,17]

$$A(\lambda) = A_{epi}(\lambda) + A_{der}(\lambda) + S(\lambda). \tag{7}$$

Using Eq. (6), Eq. (7) is rewritten as

$$\begin{aligned} A(\lambda) = {} & C_m \times \overline{l}_{epi}(\lambda, C_m) \times \varepsilon_m(\lambda) \\ & + C_{oh} \times \overline{l}_{der}(\lambda, C_{oh}, C_{dh}) \times \varepsilon_{oh}(\lambda) \\ & + C_{dh} \times \overline{l}_{der}(\lambda, C_{oh}, C_{dh}) \times \varepsilon_{dh}(\lambda) + S(\lambda), \end{aligned} \tag{8}$$

where the subscripts m, oh, and dh for C and $\varepsilon(\lambda)$ denote the melanin, oxygenated hemoglobin, and deoxygenated hemoglobin, respectively. The two functions $\overline{l}_{epi}(\lambda, C_m)$ and $\overline{l}_{der}(\lambda, C_{oh}, C_{dh})$ are the mean path length in epidermis and dermis, respectively. For light diffusely reflected from a semi-infinite medium containing absorbers, it is generally known[16,17] that the mean path length becomes shorter as the concentration of absorbers increases, while the attenuation by scattering has no change. There are also some other chromophores such as bilirubin in skin tissue, but their contribution to the absorbance spectrum is considered to be small in comparison with those of the three chromophores given here. Then we assume that the effect of other chromophores is included in $S(\lambda)$ of Eq. (8).

By using the absorbance spectrum as a response variable and the molar extinction coefficients of the three chromophores as predictor variables, the multiple regression model given by Eq. (1) can be applied to Eq. (8) as[15]

$$\begin{aligned} A(\lambda_k) = {} & a_m \times \varepsilon_m(\lambda_k) + a_{oh} \times \varepsilon_{oh}(\lambda_k) \\ & + a_{dh} \times \varepsilon_{dh}(\lambda_k) + a_0 + e(\lambda_k), \end{aligned} \tag{9}$$

where a_m, a_{oh}, a_{dh}, and a_0 are the regression coefficients, $e(\lambda_k)$ is an error component, and λ_k indicates discrete values in the wavelength range treated in the analysis. By executing the multiple regression analysis for one sample of the absorbance spectrum consisting of a p number of discrete wavelengths, one set of the four regression coefficients is obtained. When they are denoted by $\hat{a}_m$, $\hat{a}_{oh}$, $\hat{a}_{dh}$, and $\hat{a}_0$, the resultant regression equation is written as

$$\hat{A}(\lambda_k) = \hat{a}_m \times \varepsilon_m(\lambda_k) + \hat{a}_{oh} \times \varepsilon_{oh}(\lambda_k) + \hat{a}_{dh} \times \varepsilon_{dh}(\lambda_k) + \hat{a}_0, \tag{10}$$

where $\hat{A}(\lambda_k)$ is the estimated absorbance spectrum. In this case, the regression coefficient $\hat{a}_0$ is expressed by applying the relation of Eqs. (2) and (3) to Eqs. (9) and (10), as

$$\hat{a}_0 = \overline{A} - \overline{\varepsilon}_m \times \hat{a}_m - \overline{\varepsilon}_{oh} \times \hat{a}_{oh} - \overline{\varepsilon}_{dh} \times \hat{a}_{dh}, \tag{11}$$

where $\overline{A}$, $\overline{\varepsilon}_m$, $\overline{\varepsilon}_{oh}$, and $\overline{\varepsilon}_{dh}$ are the averages of $A(\lambda_k)$, $\varepsilon_m(\lambda_k)$, $\varepsilon_{oh}(\lambda_k)$, and $\varepsilon_{dh}(\lambda_k)$ over the wavelength range, or $k = 1$ to p. In this paper, we denote this part of the multiple regression analysis, MRA1.

The regression coefficients, $\hat{a}_m$, $\hat{a}_{oh}$, and $\hat{a}_{dh}$ describe the degree of contribution of each molar extinction coefficient to the absorbance spectrum and thus the three regression coefficients are closely related to the concentrations C_m, C_{oh}, and C_{dh}, respectively. Then, in Eq. (11), the value of $\hat{a}_0$ is also related to the three concentrations. As seen from the first terms in Eqs. (8) and (10), however, the regression coefficient $\hat{a}_m$ includes a factor of the mean path length in epidermis, $\overline{l}_{epi}(\lambda, C_m)$ and the value of $\hat{a}_m$ is nonlinearly related to that of C_m. This discussion applies also in the cases of $\hat{a}_{oh}$ and $\hat{a}_{dh}$ for dermis. Moreover, the regression coefficient $\hat{a}_m$ depends on the concentrations of oxygenated hemoglobin C_{oh} and deoxygenated hemoglobin C_{dh} in dermis, and $\hat{a}_{oh}$ and $\hat{a}_{dh}$ depend on C_m as well. As illustrated in Fig. 2, light incident on the skin's surface is propagated into epidermis and dermis under the scattering and absorption. Then some portion of the scattered light comes back from the dermis to the

epidermis and finally is emitted from the surface. Therefore, the increase in A_{der} according to C_{oh} and C_{dh} causes a decrease in the light scattered back to the epidermis and thus results in a decrease in A_{epi}. Similarly, an increase in A_{epi} according to C_m may result in a decrease in A_{der}. In this way, the absorbance effects in epidermis and dermis are interdependent and their contributions cannot be separated. Therefore, the absolute values of C_m, C_{oh}, and C_{dh} are not accurately determined only from $\hat{a}_m$, $\hat{a}_{oh}$, and $\hat{a}_{dh}$, respectively. For this problem, Shimada et al.[15] have proposed the use of relative changes in the absorbance spectra as the predictor variable. But the effects of nonlinearity and interdependence mentioned above still remain in their results,[16,17] and their method is limited to a small range of the change in each concentration.

The oxygen saturation of hemoglobin in dermis, SO_2, is defined by the concentrations of oxygenated and deoxygenated hemoglobin as

$$SO_2=\frac{C_{oh}}{C_{oh}+C_{dh}}=\frac{C_{oh}}{C_{th}}, \tag{12}$$

where $C_{th}=C_{oh}+C_{dh}$ is the concentration of total hemoglobin. Using the regression coefficients in Eq. (10), the estimated oxygen saturation SO_2 may be given by

$$SO_2=\frac{\hat{a}_{oh}}{\hat{a}_{oh}+\hat{a}_{dh}}=\frac{\hat{a}_{oh}}{\hat{a}_{th}}, \tag{13}$$

where $\hat{a}_{th}=\hat{a}_{oh}+\hat{a}_{dh}$. The values of $\hat{a}_{oh}$ and $\hat{a}_{dh}$ contain the above-mentioned effects. However, it is considered that those effects on the value of SO_2 are expected to be small, because the oxygen saturation is given by a ratio of the two coefficients in Eq. (13).

2.3 *Compensation for the Nonlinearity*

To compensate for the effects of nonlinearity and interdependence in MRA1, it is necessary to know the mean path length functions $\overline{l}_{epi}(\lambda,C_m)$ and $\overline{l}_{der}(\lambda,C_{oh},C_{dh})$. However, they are generally unknown and thus it is necessary to estimate the relation between the regression coefficients $\hat{a}_m$, $\hat{a}_{oh}$, $\hat{a}_{dh}$, and $\hat{a}_0$ and the three concentration values, C_m, C_{oh}, and C_{dh}. There are some general methods for treating an estimation problem like this, including a neural network and multiple regression analysis using higher-order terms. A neural network usually gives relatively good estimates, but it is rather difficult to find appropriate parameters. As described in the previous section, we employed a multiple regression analysis to evaluate the absorption spectra because of its simplicity. To keep the effective use of this method, we apply a multiple regression analysis also to the estimation of the nonlinear relation.

When the oxygen saturation is obtained by Eqs. (12) or (13), it is enough to obtain the concentration of total hemoglobin, C_{th}, instead of both C_{oh} and C_{dh}. Thus the multiple regression model in this case is expressed by the following two equations:

$$C_m^i=\mathbf{b}_m\times\hat{\mathbf{a}}^i+e_m^i, \tag{14}$$

$$C_{th}^i=\mathbf{b}_{th}\times\hat{\mathbf{a}}^i+e_{th}^i, \tag{15}$$

$$\hat{\mathbf{a}}^i=[1,\ \hat{a}_m^i,\ \hat{a}_{th}^i,\ \hat{a}_0^i,\ \hat{a}_m^i\times\hat{a}_{th}^i,\ \hat{a}_m^i\times\hat{a}_0^i,\cdots\text{higher order terms}\cdots]^t, \tag{16}$$

$$\mathbf{b}_m=[b_m^0,\ b_m^1,\ b_m^2,\cdots,\ b_m^{z-1}], \tag{17}$$

$$\mathbf{b}_{th}=[b_{th}^0,\ b_{th}^1,\ b_{th}^2,\cdots,\ b_{th}^{z-1}], \tag{18}$$

where C_m^i and C_{th}^i $(=C_{oh}^i+C_{dh}^i)$ denote the concentrations of melanin and total hemoglobin, respectively, in the medium from which the i'th absorbance spectrum sample is obtained, and e_m^i and e_{th}^i are error components. In Eq. (16), $[\cdots]^t$ represents the transposition of the vector. Here, $\hat{\mathbf{a}}^i$ expresses the vector that contains the regression coefficients estimated by MRA1 for the i'th absorbance spectrum and their higher-order terms. The number of components in this vector is assumed to be z. In Eqs. (14) and (15), $\mathbf{b}_m\times\hat{\mathbf{a}}^i$ and $\mathbf{b}_{th}\times\hat{\mathbf{a}}^i$ are the scalar product. Two coefficient vectors $\mathbf{b}_m$ and $\mathbf{b}_{th}$ are unknown, but they can be estimated by the multiple regression analysis in which C_m^i and C_{th}^i are treated as response variables and vector components of $\hat{\mathbf{a}}^i$ as predictor variables. When the estimated coefficient vectors are denoted as $\hat{\mathbf{b}}_m$ and $\hat{\mathbf{b}}_{th}$,

$$\hat{C}_m^i=\hat{\mathbf{b}}_m\times\hat{\mathbf{a}}^i, \tag{19}$$

$$\hat{C}_{th}^i=\hat{\mathbf{b}}_{th}\times\hat{\mathbf{a}}^i, \tag{20}$$

$$\hat{\mathbf{b}}_m=[\hat{b}_m^0,\ \hat{b}_m^1,\ \hat{b}_m^2,\cdots,\ \hat{b}_m^{z-1}], \tag{21}$$

$$\hat{\mathbf{b}}_{th}=[\hat{b}_{th}^0,\ \hat{b}_{th}^1,\ \hat{b}_{th}^2,\cdots,\ \hat{b}_{th}^{z-1}], \tag{22}$$

where $\hat{C}_m^i$ and $\hat{C}_{th}^i$ are the estimated values of C_m^i and C_{th}^i, respectively. We call this multiple regression analysis MRA2 in this paper.

To perform MRA2, we need a number of datasets that contain various concentrations of melanin C_m and total hemoglobin C_{th}, and the corresponding absorbance spectra. To prepare these data sets, we employed a Monte Carlo simulation for the layered skin tissue model.[18] This process, including the Monte Carlo calculation, is shown as the preparation work in Fig. 1 and its details are described in the next section. The coefficients $\hat{\mathbf{b}}_m$ and $\hat{\mathbf{b}}_{th}$ obtained from MRA2 imply vectors that convert the regression coefficients obtained in MRA1 to the concentrations of melanin and total hemoglobin, respectively, and thus we refer to them as the conversion vectors in this study. Once we determine the conversion vectors $\hat{\mathbf{b}}_m$ and $\hat{\mathbf{b}}_{th}$ in MRA2 for necessary ranges of the melanin and hemoglobin concentrations, the values of $\hat{C}_m$ and $\hat{C}_{th}$ can easily be obtained by Eqs. (19) and (20) from the regression coefficients in MRA1 without the Monte Carlo simulation.

3 Derivation of the Conversion Vectors

3.1 *Method*

To derive the conversion vectors numerically, we first calculated diffuse reflectance spectra at intervals of 10 nm in the

wavelength range from 400 to 700 nm by Monte Carlo simulation for the layered skin tissue model shown in Fig. 2. In this model, we assumed that melanosomes containing melanin and blood, including hemoglobin, are homogeneously distributed over the epidermis and dermis, respectively. The actual human skin overlies a fatty layer and muscle tissue, which have their own optical properties. The light reflected from the skin tissue is probably affected by these subcutaneous layers. However, the diffuse reflectance spectrum in the visible wavelength range is primarily governed by the epidermis and upper part of the dermis, although the near-infrared light probes those deeper layers. Thus, we mainly paid attention to the contribution of the two upper layers in the present simulation. A more realistic model that includes the subcutaneous layers should be used in the next study of this method.

We used the Monte Carlo code developed by Wang et al.,[18] in which the diffuse reflectance from multilayered tissue is calculated. This code uses the Henyey-Greenstein phase function.[19] The Monte Carlo simulation requires that each layer be characterized by the scattering coefficient $\mu_s(\lambda)$ cm^{-1}, absorption coefficient $\mu_a(\lambda)$ cm^{-1}, anisotropy factor $g(\lambda)$, refractive index $n(\lambda)$, and thickness d cm in the above-mentioned wavelength range. The absorption coefficient $\mu_a(\lambda)$ generally changes as the concentration of melanin or hemoglobin varies according to physiological conditions, whereas the other parameters may not substantially do so. Thus, values of the scattering coefficient $\mu_s(\lambda)$, anisotropy factor $g(\lambda)$, refractive index $n(\lambda)$, and thickness d were assumed to be known in the present model. In actual calculations, we input typical published values for $\mu_s(\lambda)$[20] of dermis and $g(\lambda)$[21] to both epidermis and dermis, which are provided as a function of wavelength. For a proper simulation, different values of $\mu_s(\lambda)$ should be used for the epidermis and dermis. However, the scattering coefficient of the epidermis was not available in the literature for the analyzed wavelength range. Thus, the same values were used for both epidermis and dermis.

It is said[20,21] that the difference in the scattering coefficient between epidermis and dermis is not large, although there actually is some. The effects of such a difference on the analysis should be investigated in the future when the estimation accuracy is studied. The refractive index $n(\lambda)$ is fixed to be 1.4 for the two layers over the wavelength range of 400 to 700 nm and thus is denoted simply by n in this paper. The thickness values d of epidermis and dermis were set to be 0.006 and 0.494 cm, respectively.

The absorption coefficient of the epidermis depends on the volume concentration of melanosome in epidermis, C_{mel}. We assumed that the absorption coefficient of a simple melanosome given in the literature[22] corresponds to that of epidermis in the case of $C_{mel}=100\%$. Then we derived the corresponding absorption coefficients of epidermis for ten different concentrations of $C_{mel}=1$ to 10% at intervals of 1%, by simply proportioning it to that for $C_{mel}=100\%$. The absorption coefficient of dermis depends both on the volume concentration C_b and oxygen saturation SO_2 of blood in dermis. In the same way as described earlier, the generally known absorption coefficients of oxygenated ($SO_2=100\%$) and deoxygenated ($SO_2=0\%$) blood having a 45% hematocrit were assumed to be that of dermis in the case of $C_b=100\%$.

Then the absorption coefficients of dermis were derived for five different concentrations of $C_b=0.2$, 0.4, 0.6, 0.8, and 1.0% in both cases of $SO_2=0$ and 100%. These derivations were made on 31 wavelength points at 400 to 700 nm at 10-nm intervals. In this way the combination of C_{mel}, C_b, and SO_2 took 100 different cases, from which 100 reflectance spectra were calculated. Taking into account our previous study[23] concerning the error of simulated results and calculation time, the number of incident photons was set to be 10^5 for each wavelength. The calculation time for one spectrum ranging from 400 to 700 nm with 31 wavelength points was roughly 30 min, using the Athlon CPU, 1.4 GHz. Then all the reflectance spectra were converted into the absorbance spectra by Eq. (5).

Performing MRA1 for all the absorbance spectra, 100 sets of the regression coefficients $\hat{a}_m$, $\hat{a}_{oh}$, $\hat{a}_{dh}$, and $\hat{a}_0$ were obtained. Although the absorbance spectra were calculated in the range of 400 to 700 nm, we employed the spectral data only in the range of 500 to 600 nm for MRA1 because the spectral features of melanin and hemoglobin notably appear in this wavelength range. In fact, the mean value of the proportion R^2 for 100 absorbance spectra was 0.98 ± 0.01, which means a good regression. In addition, the correlation between the molar extinction coefficient of oxygenated hemoglobin, $\varepsilon_{oh}(\lambda)$, and that of deoxygenated hemoglobin, $\varepsilon_{dh}(\lambda)$, is lower at 500 to 600 nm than in the other ranges, 400 to 500 and 600 to 700 nm. Thus, the multiple regression analysis may give a good separation between $\varepsilon_{oh}(\lambda)$ and $\varepsilon_{dh}(\lambda)$ as predictor variables. With this possibility, we expect that the oxygen saturation SO_2 may be estimated from the values of $\hat{a}_{oh}(\lambda)$ and $\hat{a}_{dh}(\lambda)$ by Eq. (13).

Finally, we performed MRA2 to obtain the conversion vectors for estimating the volume concentrations, C_{mel} and C_b, of melanosome and blood, respectively. In the analysis, the values of C_{mel}^i and C_b^i input into the i'th Monte Carlo simulation were used as the i'th response variables, while the regression coefficients $\hat{a}_m^i$, $\hat{a}_{th}^i$, and $\hat{a}_0^i$ obtained from the absorbance spectrum by the i'th Monte Carlo simulation were used as the i'th predictor variables. The number of datasets was 100, that is, $i=1$ to 100. From our preliminary estimations, it was reasonable to use components of the first and third order in the vector $\hat{\mathbf{a}}^i$ of Eq. (16) and thus the number z of components was 14. It is noted that the treatment in this section is not essentially different from the use of molar concentrations as described in the previous sections because the molar concentrations of melanin and hemoglobin are proportional to the volume concentrations of melanosome and blood, respectively. Table 1 lists components of the two conversion vectors $\hat{\mathbf{b}}_{mel}$ and $\hat{\mathbf{b}}_b$ which originally correspond to $\hat{\mathbf{b}}_m$ and $\hat{\mathbf{b}}_{th}$ in Eqs. (19) and (20), respectively. Two resultant regression equations using these vectors are expressed as

$$\hat{C}_{mel}^i=\hat{\mathbf{b}}_{mel}\times\hat{\mathbf{a}}^i, \tag{23}$$

$$\hat{C}_b^i=\hat{\mathbf{b}}_b\times\hat{\mathbf{a}}^i. \tag{24}$$

These equations with the values in Table 1 were used for the following numerical and experimental investigations in this paper.

Table 1 Components of the conversion vectors $\hat{\mathbf{b}}_{mel}$ and $\hat{\mathbf{b}}_b$ obtained from MRA2.

z	$\hat{\mathbf{a}}_i$	$\hat{\mathbf{b}}_{\mathrm{mel}}$		$\hat{\mathbf{b}}_b$	
1	1	$\hat{b}_{m\,0}$	−6.428E−01	$\hat{b}_{th\,0}$	−5.489E−02
2	$\hat{a}_{m\,i}$	$\hat{b}_{m\,1}$	1.692E+04	$\hat{b}_{th\,1}$	−6.050E+01
3	$\hat{a}_{th\,i}$	$\hat{b}_{m\,2}$	−4.542E+04	$\hat{b}_{th\,2}$	1.778E+04
4	$\hat{a}_{0\,i}$	$\hat{b}_{m\,3}$	7.356E+00	$\hat{b}_{th\,3}$	5.264E−01
5	$\hat{a}^3_{m\,i}$	$\hat{b}_{m\,4}$	2.172E+10	$\hat{b}_{th\,4}$	1.015E+09
6	$\hat{a}^3_{th\,i}$	$\hat{b}_{m\,5}$	−1.212E+16	$\hat{b}_{th\,5}$	−1.731E+14
7	$\hat{a}^3_{0\,i}$	$\hat{b}_{m\,6}$	2.340E+01	$\hat{b}_{th\,6}$	1.453E+01
8	$\hat{a}_{m\,i}\cdot\hat{a}_{th\,i}\cdot\hat{a}_{0\,i}$	$\hat{b}_{m\,7}$	5.523E+09	$\hat{b}_{th\,7}$	1.585E+09
9	$\hat{a}^2_{m\,i}\cdot\hat{a}_{th\,i}$	$\hat{b}_{m\,8}$	−1.647E+11	$\hat{b}_{th\,8}$	−6.486E+11
10	$\hat{a}^2_{m\,i}\cdot\hat{a}_{0\,i}$	$\hat{b}_{m\,9}$	5.766E+07	$\hat{b}_{th\,9}$	2.952E+06
11	$\hat{a}^2_{th\,i}\cdot\hat{a}_{m\,i}$	$\hat{b}_{m\,10}$	−3.080E+14	$\hat{b}_{th\,10}$	−3.072E+10
12	$\hat{a}^2_{th\,i}\cdot\hat{a}_{0\,i}$	$\hat{b}_{m\,11}$	5.298E+11	$\hat{b}_{th\,11}$	1.441E+11
13	$\hat{a}^2_{0\,i}\cdot\hat{a}_{m\,i}$	$\hat{b}_{m\,12}$	2.132E+03	$\hat{b}_{th\,12}$	−1.500E+04
14	$\hat{a}^2_{0\,i}\cdot\hat{a}_{th\,i}$	$\hat{b}_{m\,13}$	−6.203E+06	$\hat{b}_{th\,13}$	−1.682E+06

3.2 *Numerical Investigation*

Before our experiments, we performed a numerical investigation to verify the feasibility of the proposed method using the conversion vectors. Instead of measurements, we calculated newly diffuse reflectance spectra by using the Monte Carlo simulation as test samples. For the volume concentrations, C_{mel} and C_b, of melanosomes in epidermis and blood, respectively, having a 45% hematocrit in dermis, the same values as those used in Sec. 3.1 were again employed. With ten values of C_{mel} and five values of C_b, we had 50 different combinations. The oxygen saturation SO_2 of blood was set to be 60% for all 50 combinations. Other conditions for the simulation were fixed to be the same as those in Sec. 3.1. In this way we obtained 50 diffuse reflectance spectra and then converted them into the absorbance spectra by using Eq. (5). Figure 3 demonstrates typical absorbance spectra measured on the finger surface of a Japanese adult and calculated by the Monte Carlo simulation for $C_{mel}=3.0\%$, $C_b=0.2\%$, and $SO_2=60\%$. Measurements were made by using a multichannel spectrometer under the illumination of a halogen lamp light. In Fig. 3, the measured result shows relatively high absorbance in the shorter wavelength range, has a slight increase around 550 nm, and decreases again in the longer wavelength range. This distinctive curve is due to the well-known light-absorption properties[24,25] of melanin and hemoglobin, which are characterized by their molar extinction coefficients. The same spectral characteristics as in the measured result are seen also in the simulated one. This comparison

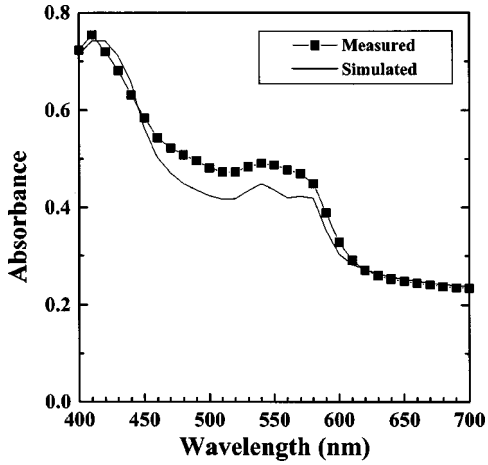

Fig. 3 Typical absorbance spectra obtained from human skin tissue and the Monte Carlo simulation.

indicates that the present calculation model is suitable for numerically simulating the diffuse reflectance spectra from human skin tissue.

Then by performing MRA1 for each absorbance spectrum, 50 sets of $\hat{a}_m$, $\hat{a}_{oh}$, $\hat{a}_{dh}$, and $\hat{a}_0$ were obtained. The mean value of the proportion R^2 was again 0.98 ± 0.01 for 50 absorbance spectra. At this point in time, the oxygen saturation SO_2 was calculated for each spectrum from Eq. (13). The mean value of SO_2 was $59.7\pm1.24\%$, which gives good agreement with the original value of 60%. To check reliability for the estimation of oxygen saturation, we performed the same investigation as above on the absorbance spectra that were calculated under the conditions of $SO_2=0$ and 100%. The mean values of SO_2 were evaluated to be 8.5 ± 1.98 and $87.0\pm2.90\%$ for the original values of 0 and 100%, respectively. This discrepancy for both cases may result from the distortion of absorbance spectra, which is due to the loss of reflection by the wavelength-dependent light scattering in the tissue. As a consequence, the absorbance spectra for $SO_2=0\%$ become not fully independent of the molar extinction coefficient $\varepsilon_{oh}(\lambda)$, although the oxygenated hemoglobin is not included in the simulation. Thus, the regression coefficient $\hat{a}_{oh}$ becomes not zero, but a certain small value in MRA1. The same discussion can be applied to the case of $SO_2=100\%$. These errors of SO_2 possibly suggest the limits of abilities of MRA1 for estimating oxygen saturation.

Figures 4(a) and 4(b) show the values of $\hat{a}_m$ and $\hat{a}_{th}(=\hat{a}_{oh}+\hat{a}_{dh})$ versus the volume concentrations, C_{mel} and C_b, of melanosomes and blood, respectively. In Fig. 4(a), the value of $\hat{a}_m$ increases nonlinearly with an increase in C_{mel}. This indicates the nonlinear relation between the absorbance of epidermis, A_{epi}, and the concentration of melanosome, C_{mel}, as described in Sec. 2.2. Moreover, the value of $\hat{a}_m$ decreases with an increase in C_b. The same tendency is also seen in the results of $\hat{a}_{th}$ shown in Fig. 4(b). These properties indicate that the absorbance of epidermis, A_{epi}, and that of dermis, A_{der}, are interdependent. On the other hand, the value of $\hat{a}_0$ (not shown here) increased with increases in both C_{mel} and C_b. Therefore it is clear that the volume concentrations of melanin and blood are not accurately determined by using only MRA1, although the regression coefficients $\hat{a}_m$,

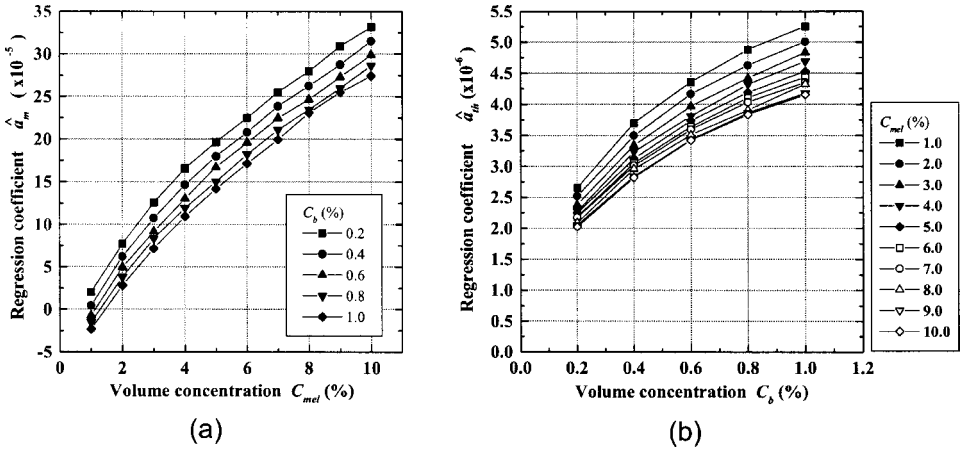

Fig. 4 Regression coefficients (a) $\hat{\mathbf{a}}_m$ and (b) $\hat{\mathbf{a}}_{th}$ versus their concentrations obtained from multiple regression analysis, MRA1.

$\hat{a}_{th}$, and $\hat{a}_0$ are related to those concentrations.

We next substituted the regression coefficients $\hat{a}_m$, $\hat{a}_{th}$, and $\hat{a}_0$ into the regression equations [Eqs. (23) and (24)] obtained in advance by MRA2 and then estimated the volume concentrations C_{mel} and C_b for each of 50 absorbance spectra, respectively. Figure 5 shows a comparison between the estimated and original values of the volume concentrations C_{mel} for melanosomes and C_b for blood. In both Figs. 5(a) and 5(b), the estimated values well agree with the original ones in given concentration ranges of C_{mel} and C_b. These results indicate the effectiveness of the method for compensation of the nonlinearity in the multiple regression analysis for skin tissue spectroscopy.

4 Experiments with Skin Tissue Phantom

4.1 *Skin Tissue Phantom*

To confirm the usefulness of the proposed method, we performed experiments using skin tissue phantoms. The phantom consists of an epidermis and a dermis layer. We prepared agar solution by diluting agar powder (Ina Food Industrial Inc., Japan) with saline at a weight ratio of 0.8%. To make the scattering condition, Intralipid 10% solution (Fresenius Kabi AB, Sweden) was added to the agar solution. The resultant solution was used as the base material for epidermis and dermis layers. The volume ratio of Intralipid 10% solution to the agar solution was one to ten. A coffee solution was introduced as a substitute for melanin into the base material, and this mixture was used to make an epidermis layer. An oxygenated dermis layer was made by adding a small amount of fully oxygenated horse blood having a 44% hematocrit to the base material, while a deoxygenated dermis layer was prepared by sufficiently dropping a $Na_2S_2O_4$-added saline solution on the surface of the oxygenated dermis layer. All these layers were hardened in various molds having the required thickness and size by being cooled at about 5.5 °C for 30 min.

The thicknesses of epidermis and dermis layers were made to be 0.1 and 0.5 cm, respectively, while the area of each layer was $2.6 \times 4.5\ \text{cm}^2$. The 0.1-cm thickness of the epidermis phantom is an order of magnitude greater than the actual epidermal thickness. In this study, however, it was difficult to make a layer thinner than 0.1 cm. To reduce the expected effects of this thickness on experimental results, then, the scattering and absorption coefficients of the epidermis phantom were controlled so that the absorbance spectrum became close to that of human skin shown in Fig. 3. The volume concentration of a coffee solution in the epidermis layer was set to be $C_c = 5.0$, 10, and 20%, while that of horse blood in the dermis layer was $C_b = 0.2$, 0.4, and 0.6%. The subscript *c*

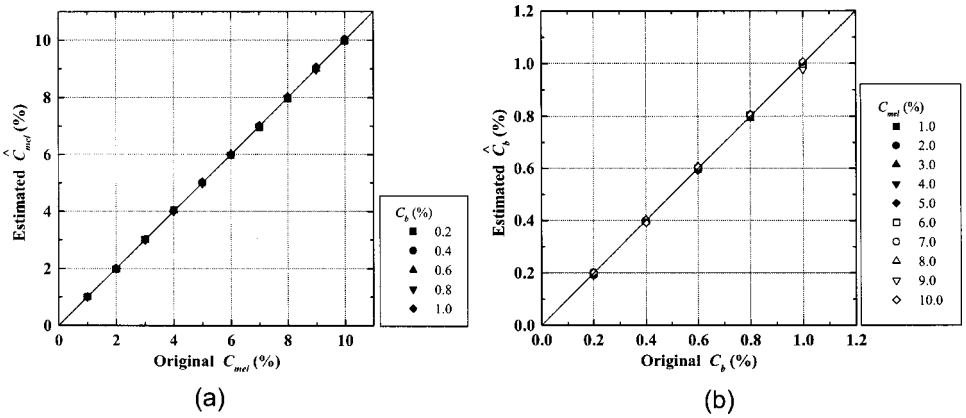

Fig. 5 Comparison of the estimated and original concentrations for (a) melanosomes and (b) blood.

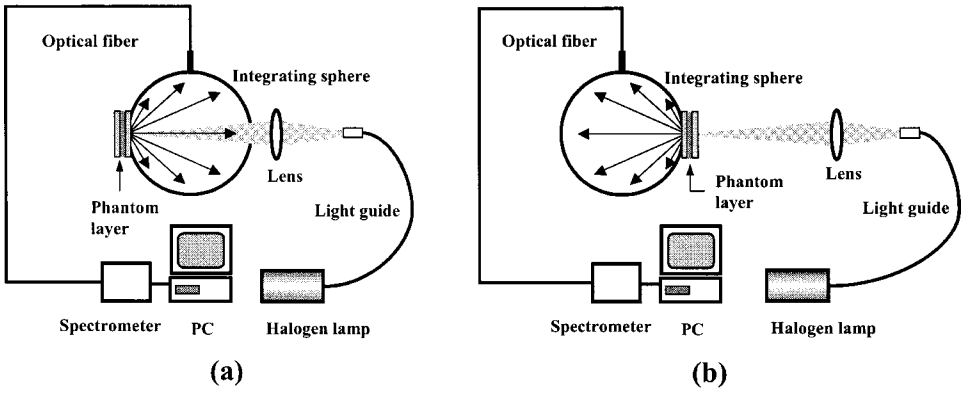

Fig. 6 Experimental setups for (a) diffuse reflectance measurements and (b) total transmittance measurements.

for the coffee concentration corresponds to *mel* for melanosome in the previous section. The oxygen saturations of blood in the oxygenated and deoxygenated dermis layers were assumed to be $SO_2 = 100$ and 0%, respectively, because both the oxygenation and deoxygenation were fully made in the above process. Finally, we built two-layered skin tissue phantoms by putting the epidermis layer on the dermis layer as the test sample.

4.2 *Method*

As preparation measurements, we first determined the absorption coefficient $\mu_a(\lambda)$ and scattering coefficient $\mu_s(\lambda)$ in 500 to 600 nm of each layer that makes up the phantoms, because $\mu_a(\lambda)$ and $\mu_s(\lambda)$ are necessary for the Monte Carlo simulation, and $\mu_a(\lambda)$ is also required to calculate the volume concentrations of coffee and blood. For this purpose, we measured diffuse reflectance and total transmittance spectra of each layer individually. Figure 6 schematically shows experimental setups for measuring diffuse reflectance spectra and total transmittance spectra. A halogen lamp light (150 W), which covers the visible wavelength range from 400 to 700 nm, illuminates the phantom layer via a light guide and lens with a spot diameter of 0.4 cm. The diameter and focal length of the lens are 5.4 and 10 cm, respectively. The layer was placed between two glass slides having a thickness of 1.0 mm and fixed at the sample holder of an integrating sphere (Labsphere Inc., RT-060-SF). The detected area of the layer was circular, with a diameter of 2.2 cm. Light diffusely reflected or transmitted from this area was received at the input face of an optical fiber probe having a diameter of 400 μm placed at the detector port of the sphere. The fiber transmits the received light into a multichannel spectrometer (Ocean Optics Inc., SD-2000), which measures reflectance or transmittance spectra in the visible wavelength range under the control of a personal computer (PC).

To determine $\mu_a(\lambda)$ and $\mu_s(\lambda)$ from measured spectra, we employed the inverse Monte Carlo method.[26] In the present study, the Monte Carlo calculation of reflectance and transmittance spectra was iterated for varying values of $\mu_a(\lambda)$ and $\mu_s(\lambda)$ until the difference between the simulated and measured spectral values decreased below a predetermined threshold. The values used in the last step of iteration were adopted as the final results. This process was carried out at intervals of 10 nm from 500 to 600 nm, and wavelength-dependent properties of $\mu_a(\lambda)$ and $\mu_s(\lambda)$ were obtained for each layer. A spectral curve for one layer was determined by averaging the results of five runs. In these calculations, the refractive index n was assumed to be 1.33 for all the layers in the whole wavelength range, and the published values[27] were used for the anisotropy factor $g(\lambda)$ of Intralipid 10%. The absorption coefficient $\mu_a(\lambda)$ varies according to the concentration of coffee or blood in each layer. Then we calculated the coefficient for a 100% volume concentration by making a linear fitting of various absorption coefficients obtained under the different concentrations given to the skin tissue phantoms. Figure 7(a) shows the resultant properties for the absorption coefficients of coffee solution $\mu_a^c(\lambda)$, oxygenated blood $\mu_a^{ob}(\lambda)$, and deoxygenated blood $\mu_a^{db}(\lambda)$, and Fig. 7(b) shows the scattering coefficient $\mu_s(\lambda)$. The scattering coefficient in Fig. 7(b) is the average value for epidermis and dermis layers.

We also need to have the conversion vectors for the skin tissue phantoms used in this study because the results of Table 1 were obtained with human skin conditions and thus were unavailable for the phantoms. We generated diffuse reflectance spectra ranging from 500 to 600 nm by using a Monte Carlo simulation with conditions of the phantoms. For this simulation, the volume concentration C_c of the coffee solution in the epidermis layer, that of blood in the dermis layer, C_b, and the oxygen saturation SO_2 of blood were set to be the same as those used for the phantoms. We thus obtained 18 different reflectance spectra from the combination of C_c, C_b, and SO_2, and then converted them into absorbance spectra by Eq. (5). Performing MRA1 and MRA2 as described in Sec. 3.1, we derived the conversion vectors and the corresponding regression equations for estimating the volume concentrations, C_c and C_b, of coffee solution and blood, respectively. The molecular weights of coffee and horse blood used for the phantoms were unknown and their molar extinction coefficients were accordingly unavailable. However, the absorption coefficient is proportional to the molar extinction coefficient. In MRA1, therefore, the absorption coefficients $\mu_a^c(\lambda)$, $\mu_a^{ob}(\lambda)$, and $\mu_a^{db}(\lambda)$ shown in Fig. 7(a) were used as the predictor variables instead of the molar extinction coefficients. The mean value of the proportion R^2 was 0.98 ± 0.01 for the 18 absorbance spectra.

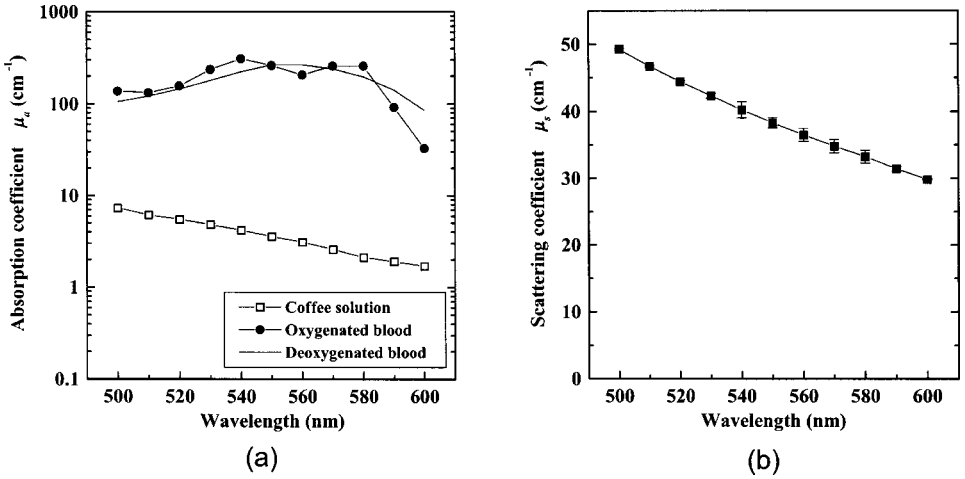

Fig. 7 Properties of (a) absorption coefficients and (b) scattering coefficient for the skin tissue phantoms used in experiments.

4.3 *Results and Discussion*

Although we made both oxygenated and deoxygenated dermis layers for the skin tissue phantom, we did not use the latter because its deoxygenated state was unstable and the optical properties of the epidermis layer may have been affected by permeation of $Na_2S_2O_4$ into the dermis layer through the epidermis layer. Hence, nine different kinds of two-layered skin tissue phantoms were made from the combination of C_c and C_b with $SO_2 = 100\%$. Using the setup of Fig. 6(a), we measured the diffuse reflectance spectra of skin tissue phantoms in the range of 400 to 700 nm and then converted them into the absorbance spectra by Eq. (5). Figure 8 shows typical absorbance spectra measured from the phantoms having different volume concentrations of the coffee solution. In Fig. 8, as the value of C_c becomes larger, the absorbance in a shorter wavelength range increases significantly in comparison with that in a longer wavelength range. This is due to the large absorption property of coffee solution in the shorter wavelength range, as expected from Fig. 7(a). The three absorbance spectra also reveal the well-known characteristic spectral curve of oxygenated blood, as shown in Fig. 7(a). These absorbance spectra of the phantom are similar to those of human skin shown in Fig. 3. Thus we conclude that the 0.1-cm thickness of the epidermis phantom had no significant effect on the present analysis, and that these skin tissue phantoms could be used successfully in our experiments.

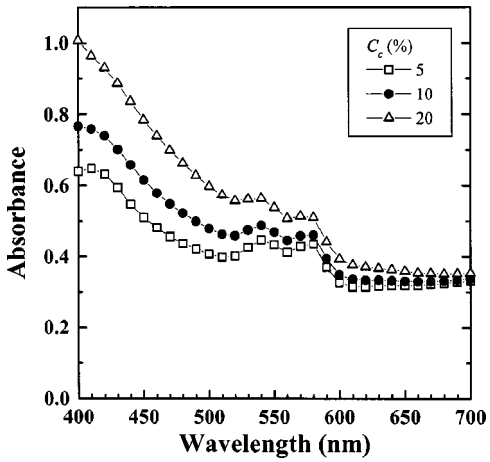

Fig. 8 Typical absorbance spectra obtained from the two-layered skin tissue phantoms.

Performing MRA1 for each absorbance spectrum measured from the skin tissue phantom, nine sets of $\hat{a}_c$, $\hat{a}_b$ $(=\hat{a}_{ob}+\hat{a}_{db})$, and $\hat{a}_0$ were obtained. Here the subscripts c, b, ob, and db correspond to m, th, oh, and dh described in Sec. 2.2, respectively. The mean value of the proportion R^2 was 0.96 ± 0.01 for the nine absorbance spectra. That of SO_2 was $87.4 \pm 7.07\%$, which resulted in underestimation with a relatively large variation. However, considering the numerical result for $SO_2 = 100\%$ discussed in Sec. 3.2, this experimental result is reasonable at present. Substituting the regression coefficients $\hat{a}_c$, $\hat{a}_b$, and $\hat{a}_0$ into the regression equations obtained by the MRA2 analysis for the skin tissue phantom in Sec. 4.2, we estimated the volume concentrations, C_c and C_b, of coffee solution and blood for each phantom, respectively. Figure 9 shows the comparison between the estimated and original values of the volume concentrations for C_c and C_b. In Fig. 9(a), the estimated value agrees with the original one for each value of C_b. The agreement between the estimated and original values is also shown in Fig. 9(b). Hence the feasibility of this method was verified by the phantom experiments. These results also demonstrate the usefulness of the skin tissue phantoms developed for this study.

5 Experiments with Human Skin Tissue

5.1 *Method*

To confirm the applicability of the present method to an *in vivo* situation, we performed time series measurements of melanin and hemoglobin on human skin tissue during cuff occlusion. A brachial cuff of a mercury sphygmomanometer (Kenzmedico Co., Ltd., Japan) was fixed around the upper arm of a Japanese adult male and pressure up to 200 mmHg was applied. Using the setup shown in Fig. 6(a), we conducted time series measurements of diffuse reflectance spectra from the surface of the forearm. Measurements were made at 2-s intervals for 14 min. One spectrum was obtained by aver-

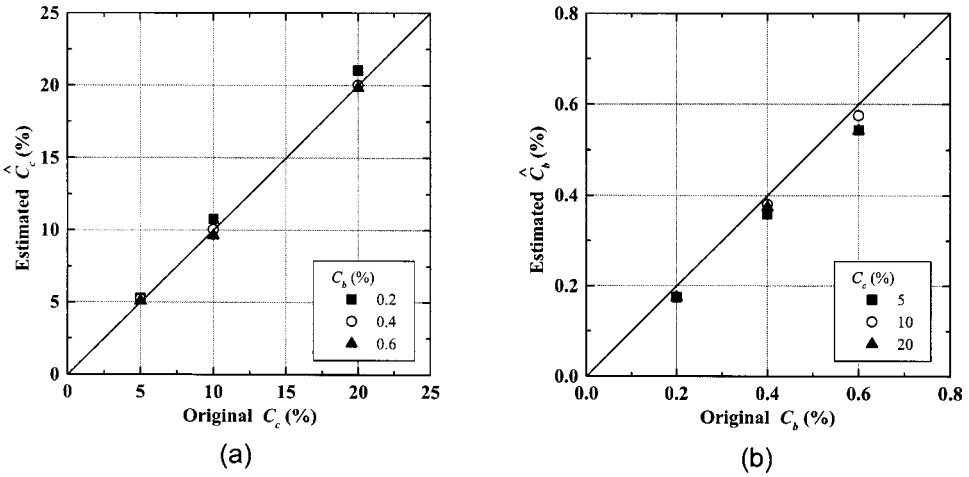

Fig. 9 Comparison of the estimated and original concentrations for (a) coffee solution and (b) blood.

aging eight runs, in which one run was made in 250 ms. We converted all the diffuse reflectance spectra into the absorbance spectra, performed MRA1 for each spectrum, and obtained time series sets of $\hat{a}_m$, $\hat{a}_{th}$, and $\hat{a}_0$. The mean value of the proportion R^2 was 0.96 ± 0.01 for all the absorbance spectra. The volume concentration of melanosomes, C_{mel}, that of blood, C_b, and the oxygen saturation SO_2 were estimated from Eqs. (23), (24), and (13), respectively, together with the conversion vectors listed in Table 1. Since these vectors were used for deriving experimental results, it should be noted that the assumptions for the scattering coefficient, anisotropy factor, refractive index, and thickness in Sec. 3.1 were applied to these human measurements.

5.2 *Results and Discussion*

Figure 10 shows the time course of C_{mel}, C_b, and SO_2 during the cuff occlusion test. Each temporal variation is plotted at every 10 sec. Before the cuff occlusion (between -140 and 0 s), the oxygen saturation ranges from 51.6 to 60.3%, which agrees with the results reported in the literatures.[3,4,6] The mean value of C_b is $0.24 \pm 0.01\%$, which is fairly close to a general example of the volume concentration of blood in dermis, $C_b = 0.2\%$, assuming that the blood is uniformly distributed. Typical ranges for the volume concentration of melanosomes in epidermis have been reported:[28] $C_{mel} = 1$ to 3% for light-skinned Caucasians, 11 to 16% for Mediterranean types, and 18–43% for darkly pigmented Africans. Considering that the subject in this experiment was a relatively light-skinned Japanese, the mean value of $C_{mel} = 4.6 \pm 0.02\%$ is acceptable.

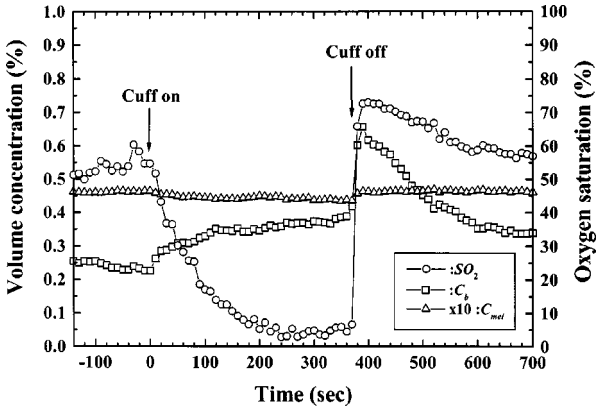

Fig. 10 Time course of concentration of melanosomes, C_{mel}, blood, C_b, and oxygen saturation SO_2, during the cuff occlusion.

During the cuff occlusion (between 0 and 370 s), the value of SO_2 shows the well-known deoxygenation curve in which the oxygen saturation falls exponentially and approaches zero. On the other hand, the value of C_b increases slowly. This change in C_b probably has a physiological cause in that during the occlusion the venous outflow is reduced more than the arterial inflow. After the cuff was released (between 370 and 700 s), both SO_2 and C_b increased sharply and then gradually returned to the values before the occlusion. These changes in SO_2 and C_b may be due to the postocclusion reactive hyperemia and oxygenation, and recovery of blood circulation. In spite of the dramatic change in SO_2 and C_b, the value of C_{mel} remains almost unchanged during measurements. This constancy of C_{mel} indicates that the interdependence between the absorbance of epidermis and that of dermis is effectively compensated by the present method. In this way, physiological conditions of human skin tissue were successfully monitored *in vivo* by using the proposed method.

However, this method requires different conversion vectors because the target tissue will have different scattering properties and thicknesses. Therefore, alternative conversion vectors must be prepared by Monte Carlo simulation whenever a target with different conditions is measured. In such a case, it may take about 12 h to generate 100 samples of reflectance spectra and to determine the conversion vectors by means of the Athlon CPU, 1.4 GHz, for example. There may be a possible approach to reduce this computational burden. Reflectance spectra of 100 samples are calculated in advance with typical scattering, absorbing, and geometric conditions. In using the present method, they are referenced as the standard set of spectra and may be modified according to deviations from the original (typical) values in those conditions when a new target tissue is measured, instead of recalculations of reflectance spectra. We consider that this approach is worth studying in future work. In addition, the problem of estimation

errors for $SO_2 = 0$ and 100% described in Sec. 3.2 still remains unsolved. These errors may be reduced if the value of SO_2 is calculated, not from the values of $\hat{a}_{oh}$ and $\hat{a}_{dh}$, but from that of $\hat{C}_{oh}$ and $\hat{C}_{dh}$. It is possible to obtain the regression equations needed for deriving $\hat{C}_{oh}$ and $\hat{C}_{dh}$ by performing MRA2. This subject will be examined in the near future.

6 Conclusion

A new method has been proposed for estimating the concentrations of melanin and hemoglobin, and oxygen saturation in human skin tissue. A multiple regression analysis based on the modified Lambert-Beer law was successfully used to determine the regression coefficients relating to the concentration of melanin and blood. Nonlinearity between the regression coefficients and the melanin and blood concentrations was compensated by using conversion vectors derived from Monte Carlo simulations. The potential of this method was verified by Monte Carlo simulation and phantom experiments using two-layered skin tissue models. The results of *in vivo* experiments presented expected variations in the melanin and blood concentrations and the oxygen saturation in human skin during cuff occlusion. At present, this method relies on typical values published in the literature for the scattering coefficient, anisotropy factor, refractive index, and thickness. It is thus necessary to evaluate how a change in these values affects the estimated results. It is also desirable to combine this method with other measurement techniques that provide some or all of the above four quantities, for example, optical coherence tomography.

Acknowledgment

Part of this work was supported by the research grant of CASIO Science Promotion Foundation, Japan.

References

1. J. B. Dawson, D. J. Barker, D. J. Ellis, E. Grassam, J. A. Cotterill, G. W. Fisher, and J. W. Feather, ''A theoretical and experimental study of light absorption and scattering by *in vivo* skin,'' *Phys. Med. Biol.* **25**, 695–709 (1980).
2. J. W. Feather, M. H.-Saffar, G. Leslie, and J. B. Dawson, ''A portable scanning reflectance spectrophotometer using visible wavelengths for the rapid measurement of skin pigments,'' *Phys. Med. Biol.* **34**, 807–820 (1989).
3. D. K. Harrison, S. D. Evans, N. C. Abbot, J. S. Beck, and P. T. McCollum, ''Spectrophotometric measurements of haemoglobin saturation and concentration in skin during the tuberculin reaction in normal human subjects,'' *Clin. Phys. Physiol. Meas.* **13**, 349–363 (1992).
4. D. J. Newton, D. K. Harrison, C. J. Delaney, J. S. Beck, and P. T. McCollum, ''Comparison of macro- and maicro-lightguide spectrophotometric measurements of microvascular haemoglobin oxygenation in the tuberculin reaction in normal human skin,'' *Physiol. Meas.* **15**, 115–128 (1994).
5. V. P. Wallace, D. C. Crawford, P. S. Mortimer, R. J. Ott, and J. C. Bamber, ''Spectrophotometric assessment of pigmented skin lesion: methods and feature selection for evaluation of diagnostic performance,'' *Phys. Med. Biol.* **45**, 735–751 (2000).
6. A. A. Stratonnikov and V. B. Loschenov, ''Evaluation of blood oxygen saturation *in vivo* from diffuse reflectance spectra,'' *J. Biomed. Opt.* **6**, 457–467 (2001).
7. M. S. Patterson, B. Chance, and B. C. Wilson, ''Time resolved reflectance and transmittance for the noninvasive measurement of tissue optical properties,'' *Appl. Opt.* **28**, 2331–2336 (1989).
8. J. B. Fishkin, O. Coquoz, E. R. Anderson, M. Brenner, and B. J. Tromberg, ''Frequency-domain photon migration measurements of normal and malignant tissue optical properties in a human subject,'' *Appl. Opt.* **36**, 10–20 (1997).
9. T. J. Farrell, M. S. Patterson, and B. Wilson, ''A diffusion theory model of spatially resolved, steady-state diffuse reflectance for the noninvasive determination of tissue optical properties *in vivo*,'' *Med. Phys.* **19**, 879–888 (1992).
10. S. L. Jacques, A. Gutsche, J. A. Schwartz, L.-H. Wang, and F. K. Tittel, ''Video reflectometry to specify optical properties of tissue *in vivo*,'' in *Medical Optical Tomography: Functional Imaging and Monitoring*, Vol. IS11, pp. 211–226, SPIE Institute Series, SPIE, Bellingham, WA (1993).
11. L. Wang and S. L. Jacques, ''Use of a laser beam with an oblique angle on incidence to measure the reduced scattering coefficient of a turbid medium,'' *Appl. Opt.* **34**, 2362–2366 (1995).
12. A. Kienle, L. Lilge, M. S. Patterson, R. Hibst, R. Steiner, and B. C. Wilson, ''Spatially resolved absolute diffuse reflectance measurements for noninvasive determination of the optical scattering and absorption coefficients of biological tissue,'' *Appl. Opt.* **35**, 2304–2314 (1996).
13. S.-P. Lin, L.-H. Wang, S. L. Jacques, and F. K. Tittel, ''Measurement of tissue optical properties by the use of oblique-incidence optical fiber reflectometry,'' *Appl. Opt.* **36**, 136–143 (1997).
14. N. Tsumura, H. Haneishi, and Y. Miyake, ''Independent-component analysis of skin color image,'' *J. Opt. Soc. Am. A* **16**, 2169–2176 (1999).
15. M. Shimada, Y. Masuda, Y. Yamada, M. Itoh, M. Takahashi, and T. Yatagai, ''Explanation of human skin color by multiple linear regression analysis based on the modified Lambert-Beer law,'' *Opt. Rev.* **7**, 348–352 (2000).
16. M. Shimada, Y. Yamada, M. Itoh, and T. Yatagai, ''Melanin and blood concentration in human skin studied by multiple regression analysis: experiments,'' *Phys. Med. Biol.* **46**, 2385–2395 (2001).
17. M. Shimada, Y. Yamada, M. Itoh, and T. Yatagai, ''Melanin and blood concentration in human skin studied by multiple regression analysis: assessment by Monte Carlo simulation,'' *Phys. Med. Biol.* **46**, 2397–2406 (2001).
18. L.-H. Wang, S. L. Jacques, and L.-Q. Zheng, ''MCML-Monte Carlo modeling of photon transport in multi-layered tissues,'' *Comput. Methods Programs Biomed.* **47**, 131–146 (1995).
19. L. G. Henyey and J. L. Greenstein, ''Diffuse radiation in the galaxy,'' *Astrophys. J.* **93**, 70–83 (1941).
20. S. L. Jacques, ''Origins of tissue optical properties in the UVA, Visible, and NIR region,'' in OSA TOPS on Advances in Optical Imaging and Photon Migration, R. R. Alfano and J. G. Fujimoto, Eds., Vol. 2, pp. 364–369, Optical Society of America, Washington, DC (1996).
21. M. J. C. van Gemert, S. L. Jacques, H. J. C. M. Sterenborg, and W. M. Star, ''Skin Optics,'' *IEEE Trans. Biomed. Eng.* **36**, 1146–1154 (1989).
22. S. L. Jacques and D. J. McAuliffe, ''The melanosome: threshold temperature for explosive vaporization and internal absorption coefficient during pulsed laser irradiation,'' *J. Photochem. Photobiol., A* **53**, 769–775 (1991).
23. I. Nishidate, Y. Aizu, and H. Mishina, ''Estimation of absorbing components in a local blood layer embedded in the turbid media on the basis of visible to near-infrared (VIS-NIR) reflectance spectra,'' *Opt. Rev.* **10**, 427–435 (2003).
24. T. Sarna and R. C. Sealy, ''Photoinduced oxygen consumption in melanin systems. Action spectra and quantum yields for eumelanin and synthetic melanin,'' *Photochem. Photobiol.* **39**, 69–74 (1984).
25. R. P. Crippa, V. Cristofoletti, and N. Romeo, ''A band model for melanin deduced from optical absorption and photoconductivity experiments,'' *Biochim. Biophys. Acta* **538**, 164–170 (1978).
26. A. Roggan, M. Friebel, K. Dörschel, A. Hahn, and G. Muller, ''Optical properties of circulating human blood in the wavelength range 400–2500 nm,'' *J. Biomed. Opt.* **4**, 36–46 (1999).
27. H. J. van Staveren, C. J. M. Moes, J. Marle, S. A. Prahl, and M. J. C. Gamert, ''Light scattering in Intralipid-10% in the wavelength range of 400–1100 nm,'' *Appl. Opt.* **30**, 4507–4514 (1991).
28. S. L. Jacques, R. D. Glickman, and J. A. Schwartz, ''Internal absorption coefficient and threshold for pulsed laser disruption of melanosomes isolated from retinal pigment epithelium,'' *Proc. SPIE* **2681**, 468–477 (1996).